

Volume and Freshwater Flux Observations from Nares Strait to the West of Greenland at Daily Time Scales from 2003 to 2009

ANDREAS MÜNCHOW

University of Delaware, Newark, Delaware

(Manuscript received 19 May 2015, in final form 20 July 2015)

ABSTRACT


Time series observations of velocity, salinity, pressure, and ice draft provide estimates of advective fluxes in Nares Strait from 2003 to 2009 at daily to interannual time scales. Velocity and salinity are integrated across the 36-km-wide and 350-m-deep channel for two distinct multiyear periods of sea ice cover. These observations indicate multiyear mean fluxes that range from 0.71 ± 0.09 to 1.03 ± 0.11 Sverdrups (Sv; $1 \text{ Sv} \equiv 10^6 \text{ m}^3 \text{ s}^{-1} = 31\,536 \text{ km}^3 \text{ yr}^{-1}$) for volume and from 32 ± 5.7 to 54 ± 9.3 mSv ($1 \text{ mSv} \equiv 10^3 \text{ m}^3 \text{ s}^{-1}$) for oceanic freshwater relative to a salinity of 34.8 for the first (2003–06) and second (2007–09) periods, respectively. Advection of ice adds another 8 ± 2 mSv or $260 \pm 70 \text{ km}^3 \text{ yr}^{-1}$ to the freshwater export. Flux values are larger when the sea ice is mobile all year. About 75% of the oceanic volume and freshwater flux variability is correlated at daily to interannual time scales. Flux variability peaks at a 20-day time scale and correlates strongly with along-channel pressure gradients ($r^2 = 0.68$). The along-channel pressure gradient peaks in early spring when the sea ice is often motionless with higher sea level in the Arctic that drives the generally southward ocean circulation. Local winds contribute only when the sea ice is mobile, when they explain 60% of its variance ($r^2 = 0.60$). Observed annual to interannual change in the duration of motionless sea ice conditions impacts ocean stratification and freshwater flux, while seasonal variations are small.

1. Introduction

The Canadian Archipelago and Fram Strait constitute the two pathways for the exchange of water and ice between the Arctic and Atlantic Oceans. Arctic outflows via these pathways return freshwater to the North Atlantic that was evaporated from tropical oceans, transported by the atmosphere, and delivered to the Arctic Ocean via precipitation, terrestrial runoff, and inflow from the North Pacific (Emile-Geay et al. 2003). This study focuses on the throughflows west of Greenland where Nares Strait is a major conduit of southward flux into Baffin Bay (Münchow et al. 2015) and from there via Davis Strait (Curry et al. 2014) onto the Labrador shelf and slope of the Atlantic Ocean (Khaliwala et al. 1999). Fluxes through Nares Strait reflect the impacts of freshwater

storage and release associated with the Beaufort gyre (Proshutinsky et al. 2009; Timmermans et al. 2011), diminishing sea ice in the Arctic (Parkinson and Cavalieri 2008; Stroeve et al. 2012), disintegrating ice shelves of northern Canada (Copland et al. 2007), and potentially surging glaciers of northern Greenland (Rignot and Steffen 2008; Johnson et al. 2011). Models of global climate projections are sensitive to the parameterizations of both processes and pathways of freshwater flux from the Arctic to the North Atlantic (Holland et al. 2007; Curry and Mauritzen 2005).

The pack ice and upper Arctic Ocean are a reservoir of nearly $100\,000 \text{ km}^3$ of freshwater (Aagaard and Carmack 1989; Haine et al. 2015). This volume represents about 15 yr of local input that buffers imbalances in the annual freshwater budget. Conversely, the reservoir can deliver large pulses of freshwater to the Atlantic. The factors influencing storage and release relate to the wind stress curl over the central Arctic (Proshutinsky et al. 2009) that in ice-covered seas is modified by sea ice. Changes in the spatial distribution of sea ice and wind stress curl contribute to a myriad of observed Arctic changes such as the shift in the boundary between Atlantic- and Pacific-derived waters (Morison et al. 1998); a shift in

 Denotes Open Access content.

Corresponding author address: Andreas Münchow, College of Earth, Ocean, and Environment, University of Delaware, 112A Robinson Hall, Newark, DE 19716.
E-mail: muenchow@udel.edu

DOI: 10.1175/JPO-D-15-0093.1

the position of the transpolar drift (Rigor et al. 2002); retreat and return of the cold halocline in the Eurasian basin (Alkire et al. 2007); reduced pack ice (Lindsay et al. 2009); changes in freshwater content (Polyakov et al. 2008; Rabe et al. 2014); increased runoff into the Eurasian sector (Peterson et al. 2002); and many more (White et al. 2007).

Meanwhile, Arctic freshwater export impacts downstream deep-water formation zones in the Greenland and Labrador Seas. A prominent example is the Great Salinity Anomaly, a freshwater lens of Arctic origin that propagated as a coherent feature around the subpolar gyre of the North Atlantic Ocean (Belkin 2004). Arctic freshwater signal were detected in deep waters both in the North Atlantic by Curry and Mauritzen (2005) and in adjacent basins such as Baffin Bay by Zweng and Münchow (2006). The propagation of these freshwater signals is linked to atmospheric variations by both models and observations (Sundby and Drinkwater 2007; Hurrell and Deser 2009). Furthermore, models predict that increased surface freshening in the Greenland and Labrador Seas will slow down the global meridional overturning circulation (Koenigk et al. 2007). Possible early evidence for such slowing has been reported by Bryden et al. (2005), although Wunsch and Heimbach (2006) suggests that aliasing may explain some of the observed trends in hydrographic observations.

The potential climate impact of Arctic freshwater export motivates observational studies in the central Arctic (Proshutinsky et al. 2009) as well as its gates to the Pacific (Woodgate et al. 2012) and the Atlantic Oceans via Fram Strait (Rabe et al. 2013; de Steur et al. 2009) and Davis Strait (Curry et al. 2014). Numerical models often compare their predictions against this metric (Jahn et al. 2012) as it connects high-latitude physical forcing to midlatitude environmental responses (Greene et al. 2008). The respective roles of freshwater flux to the west and east of Greenland features in most modern large-scale coupled ice, ocean, atmospheric circulation studies (Holland et al. 2007). For similar reasons, McGeehan and Maslowski (2012), Wekerle et al. (2013), and Lu et al. (2014) all simulate decadal variability of freshwater flux through the Canadian Arctic Archipelago. The models generally agree with observations for integrated linear properties such as freshwater content, volume flux, and sea level; however, model and data diverge on nonlinear products of properties such as freshwater flux that require both velocity and salinity estimates.

Efforts to compile estimates of various component fluxes through the Arctic gateways have generally asserted that the freshwater fluxes east and west of Greenland are similar in size (Beszczynska-Möller et al.

2011). Dickson et al. (2007) cautioned, however, that the fluxes to the east and west of Greenland are potentially unsteady and may impact the overturning circulation differently. More specifically, the impact of the Arctic freshwater outflow on the global overturning circulation depends on whether (i) it is spread to depth in the Atlantic Ocean via the overflow system of Nordic Seas east of Greenland (Dickson et al. 2002), (ii) it is inserted at the surface of the North Atlantic via eddies, or (iii) it is trapped on continental shelves (Khatiwala et al. 1999; Myers 2005). Koenigk et al. (2007) predict a likely 48% increase in the freshwater flux through the Canadian Archipelago on centennial time scales, compared to only a 3% increase through Fram Strait, as a result of a much diminished Arctic ice cover (Stroeve et al. 2011) and thickness (Kwok and Rothrock 2009).

Direct current measurements are sparse within the Canadian Archipelago (Melling et al. 2008). Strong and persistent currents have been measured in the Robeson (Sadler 1976) and Kennedy Channels (Münchow et al. 2007) of Nares Strait as well as in Smith Sound (Melling et al. 2001) and in Barrow Strait (Peterson et al. 2012). Mean currents in the direction of Kelvin wave propagation are often intensified near the surface adjacent to channel boundaries (LeBlond 1980; Münchow et al. 2007).

Münchow and Melling (2008) provided initial descriptions and analyses of ocean currents in Nares Strait from 2003 to 2006. Focusing on depth-averaged properties only, they found a steady sectionally averaged mean flow of about 0.06 m s^{-1} to the south that corresponds to a volume flux of 0.72 ± 0.11 Sverdrups (Sv; $1 \text{ Sv} \equiv 10^6 \text{ m}^3 \text{ s}^{-1}$). This study extends this work by (i) introducing a more complete 2003–09 record; (ii) extending velocity observations to the surface using new estimates of ice velocity; (iii) presenting full-section estimates of volume and freshwater flux; and (iv) demonstrating that both volume and freshwater flux correlate strongly with each other and the along-channel pressure gradients.

2. Study area, data, and methods

Nares Strait connects the Lincoln Sea of the Arctic to Baffin Bay of the Atlantic Ocean (Fig. 1). Across a 36-km-wide section, an array of 75-kHz acoustic Doppler current profilers (ADCP) of Teledyne RD Instruments was deployed in 2003 at the bottom at depths ranging from 170 m off Greenland to 370 m in the center of Kennedy Channel near 80.5°N (Fig. 2). Münchow and Melling (2008) describe mooring details and discuss vertically averaged properties at tidal to interannual time scales for five instruments recovered in 2006. A second deployment of these five ADCPs in 2007 was recovered

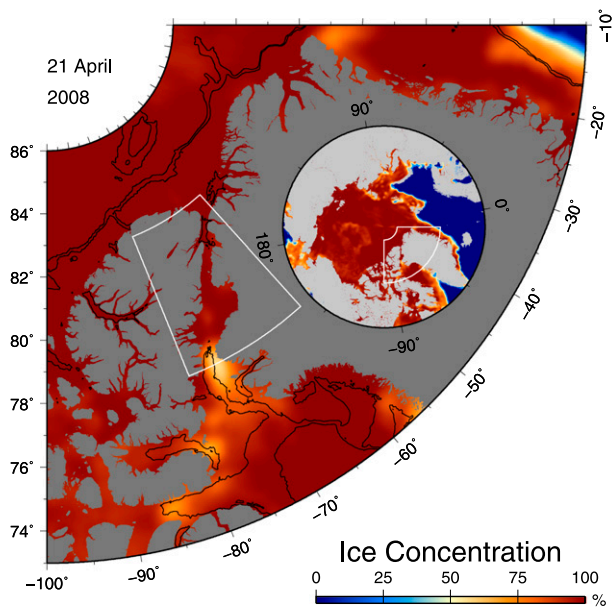


FIG. 1. Map of the study area off north Greenland with Nares Strait in the center. The insert shows the Arctic and adjacent North Atlantic Oceans. Colors indicate sea ice concentrations on 21 Apr 2008 as seen from SSM/I satellite, while black contours are 500- and 1000-m isobaths.

without losses in 2009. Ocean currents were sampled in bursts for 5 min every half hour in 50 separate 8-m vertical bins (Münchow et al. 2006). Beam angles of 20° from the vertical prevent reliable water velocity observations near the surface from 6% of the water depth plus one bin depth. For the deepest (shallowest) mooring at 366 m (157 m), this gives a surface data loss of about 30 m (18 m). Additional surface data loss relates to a time-variable ice draft that reaches 5–10 m as well as the absence of scatters under the ice in winter. Tidal oscillations are removed from the record via harmonic analysis prior to application of a Lanczos raised cosine filter with a half-power point near 34 h (Münchow and Melling 2008). Table 1 provides salient mooring details.

Data from bottom-mounted ADCP moorings are also used to estimate ice velocity from water-tracking pings. Following methodology developed independently by Melling et al. (1995) and Visbeck and Fischer (1995), I use the Doppler shift from the vertical bin that contains a near-surface maximum of acoustic backscatter. This maximum is distinct across all four beams in the presence of level ice when all four acoustic beams track the same piece of ice. The resulting estimates were filtered and subsampled at 3-h intervals to retain the tides while reducing noise. Ice draft measurements originate from an ASL Environmental Sciences ice profiling sonar to distinguish an ice surface from open water (Melling 1998). Two sonars were moored adjacent to ADCPs at

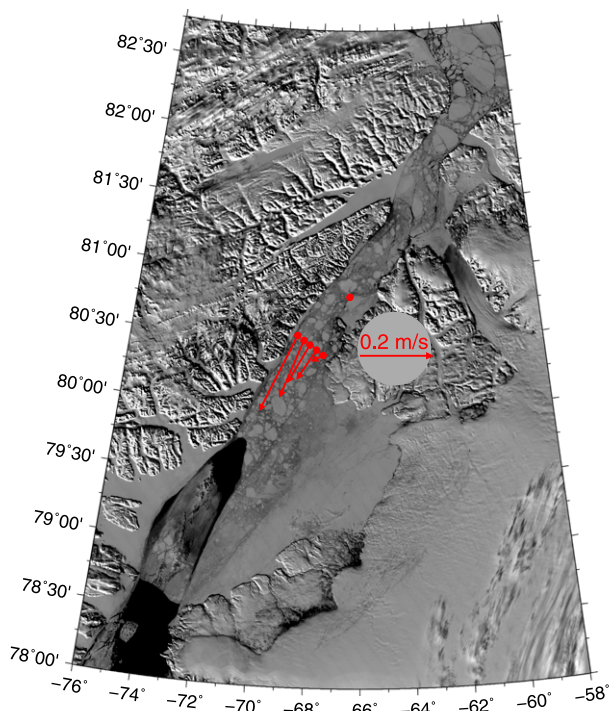


FIG. 2. Nares Strait with 5-day filtered current vectors at the mooring section in Kennedy Channel centered in time on 21 Apr 2008 overlaid on a MODIS-Terra image of surface reflectance sensed that day. A low sun angle illuminates mountainous terrain of Ellesmere Island in the west and Greenland in the east. Open water or thin ice is indicated by the black color near 74° W.

100-m depth and measured ice draft to within 0.1 m (P. Ryan 2015, personal communication).

Separate moorings held four SeaBird SBE37SM Microcats each that measured conductivity and temperature (C/T) to estimate salinity above 200 m as well as pressure at two vertical locations from which mooring motions can be inferred. Rabe et al. (2010, 2012) describes details of the mooring design, location, and data processing for the 2003–06 period that I here apply to the 2007–09 period. Additional C/T sensors were placed 3 m above the bottom at ADCP mooring locations (Münchow et al. 2011).

Bottom pressure observations originate from a Digiquartz pressure sensor of ParaScientific, Inc., that is accurate to within 0.2 mbar (Münchow and Melling 2008) and was deployed in a shallow bay of Foulke Fjord, Greenland (78.30° N, 72.57° W), at the southern end of Nares Strait. Data from a surface tide gauge at Alert, Canada (82.49° N, 75.80° W), were used and corrected for the inverted barometer effect in order to estimate the bottom pressure gradient along Nares Strait by subtracting corrected Alert from Foulke Fjord bottom pressure estimates.

Wind data used here originate from numerical simulations described by Samelson and Barbour (2008). The

TABLE 1. Mooring locations and records. Distance is measured from the coast of Ellesmere Island.

Name	Year	Longitude (°W)	Latitude (°N)	Depth (m)	Distance (km)	Bins	Record (days)
KS02	2003–06	68.8744	80.5538	302	2.2	32	1103
KS10	2003–06	67.9296	80.4388	299	23.9	32	1105
KS12	2003–06	67.6709	80.4092	263	29.6	27	1104
KS14	2003–06	67.4458	80.3884	157	34.4	15	1103
KS04	2007–09	68.7393	80.5378	366	5.2	39	718
KS06	2007–09	68.4555	80.5038	358	11.7	38	718
KS08	2007–09	68.1850	80.4715	356	17.8	38	719
KS10	2007–09	67.8930	80.4355	294	24.6	31	719
KS12	2007–09	67.5927	80.3993	228	31.5	23	717

Nares Strait model uses boundary conditions from operational global meteorological forecast models via three-step nesting procedures at 54-, 18-, and finally 6-km resolutions. The 6-km model provides realistic 36-h predictions of wind fields for Nares Strait at hourly intervals. I use model output from a single grid point near the center of the moorings section near 80.5°N latitude and 68°W longitude.

I use remotely sensed surface conditions from daily observations of microwave SSM/I and optical MODIS satellites. The SSM/I data used are sea ice concentrations obtained from NSIDC archives at 25-km resolution (Steffen and Schweiger 1991), while MODIS data are surface reflectance at 865 nm obtained from NASA's Goddard Space Flight Center at 250-m resolution.

3. Sea ice conditions

Nares Strait is covered by sea ice for most of the year (Fig. 1). From July to November the ice is mobile, while from December to June it is generally landfast as a result of ice arches that form at the northern entrance at 83°N and southern exit at 78°N (Kwok et al. 2010). Figure 2 shows an optical MODIS–Terra satellite image from 21 April 2008 at 250-m spatial resolution. The low sun angle naturally illuminates the high mountainous terrain of Ellesmere Island, Canada, in the west and Greenland in the east. Black ocean areas to the south of 80°N indicate open water or very thin ice as an ice bridge blocks all ice motion to the north. The ocean under the ice moves, however, as indicated by low-pass filtered current vectors observed at the mooring locations on 21 April 2008. The ocean under the ice moves southward at speeds reaching 0.2 m s^{-1} , while the ice above it is stationary.

Almost exactly a year later on 22 April 2009, Fig. 3 shows a different winter distribution of the sea ice in Nares Strait. No southern ice bridge formed this year; however, a northern ice arch prevents advection of ice into the channel that is covered by thin mobile ice or open water. Note that surface currents are again

southward. The largest downstream velocities at this time occur in the center of the channel reaching 0.3 m s^{-1} , while the year prior the largest flow was adjacent to the western coast. The presence of mobile versus immobile and landfast ice impacts dynamics, volume, and fresh-water flux.

4. Circulation

Measuring ocean currents within 30 m of an ice–ocean interface challenges available technologies. For example, the bottom-mounted ADCPs in the 350-m-deep Nares Strait measure velocity reliably only to within 30- or 40-m

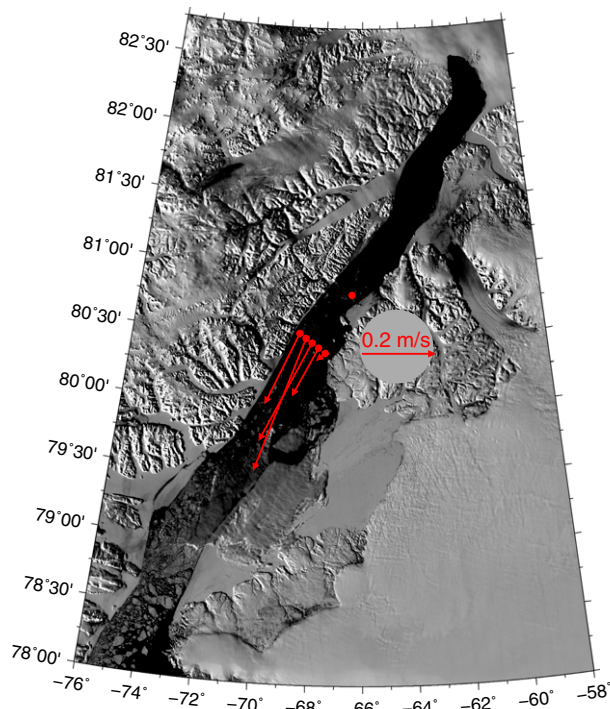


FIG. 3. As in Fig. 3, but for 22 Apr 2009. The black color indicates Nares Strait to be covered by open water or thin ice due to a northern ice arch at 60°W.

of the surface on account of variable ice thickness, lack of scatterers, and acoustic sidelobe interference from the ice surface that mask the water column signal near the surface. The signals reflected back to the ADCP transducers from the ice surface, however, allow direct estimation of an ice surface velocity (Melling et al. 1995). I combine this ice surface velocity with subsurface water velocities to interpolate velocity data across the unmeasured 30–40-m-thick surface with a dynamically motivated vertical shear model introduced by Münchow et al. (2007) and developed further here. These data and methods will provide for accurate volume and freshwater flux estimates at daily to interannual time scales.

a. Ocean velocity

Figure 4 shows vertically averaged ocean currents as the record mean (arrow) and subtidal variability (filled ellipse) for the 2003–06 and 2007–09 observational periods that are also summarized in Table 2. Record-mean flows are always to the south. The strongest mean currents occur within 10 km off the Ellesmere Island coast in the west. In contrast, I find the largest variability off Greenland where the ellipse is long and slender (Münchow and Melling 2008).

The depth-dependent flow is always to the south and statistically significantly different from zero at 95% confidence (Fig. 5). Veering occurs below 200-m depth toward the bottom and above 30 m toward the surface. Record-mean currents are identical for the two periods within their confidence interval except for the near-surface flow that is significantly stronger during the 2007–09 relative to the 2003–06 period. Figure 6 shows the time series of wind and ocean current vectors within 115 m of the surface. Winds are persistent from the north and exceed 10 m s^{-1} frequently. Ocean currents are detided and low-pass filtered. Wind and 35-m currents have strong seasonality with the strongest southward wind and currents occurring in January and February with weaker southward flow and northward winds in June and July. Strong winds and ocean currents along with mobile sea ice will result in large values for both volume and freshwater flux during the 2007–09 period. In contrast, during the 2003–06 period persistent ice arches form to the south of our study area and shut down all ice motion and atmospheric momentum transfer to the ocean for 5 to 8 months each year (Kwok et al. 2010).

b. Ice velocity

Figures 7 and 8 show time series of the along-channel ice velocities along with the ice draft for the 2003–06 and 2007–09 periods, respectively. In combination these data document the passage of rafted ice during the mobile season as well as the slowly growing level ice during the

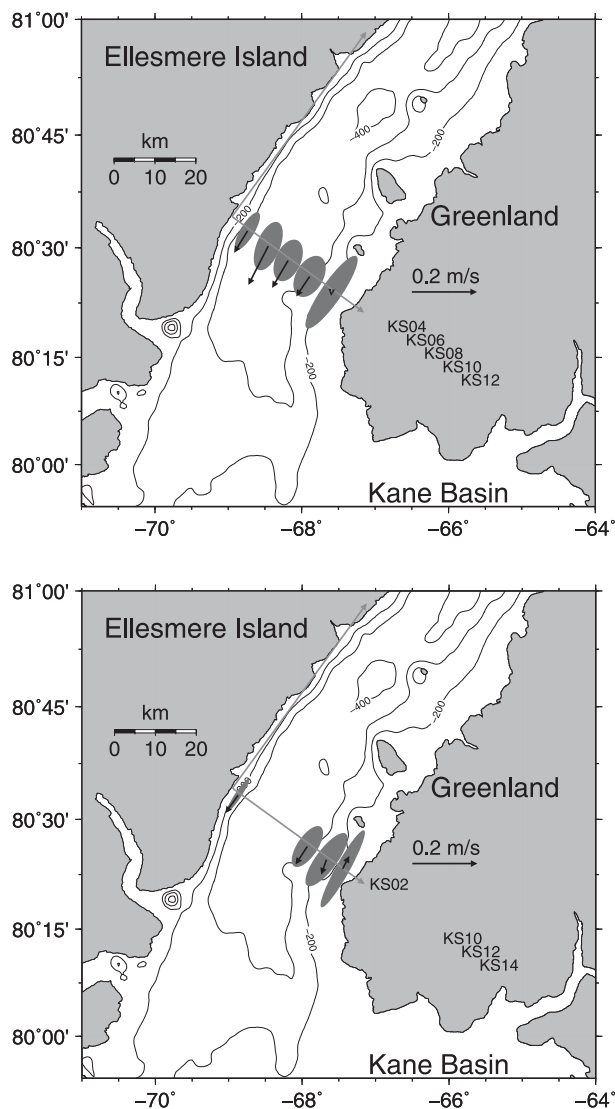


FIG. 4. Record-mean and principal components of vertically averaged ocean current vectors for the (top) 2007–09 and (bottom) 2003–06 periods. The coordinate system for along- and across-channel directions is indicated with an origin on the Ellesmere Island coastline. Contours are 200-, 300-, and 400-m bottom depth. See Fig. 2 for locations. The Kennedy Section (KS) stations displayed are indicated.

winter periods when ice motion is small. During the summer, ice motions frequently exceed 1 m s^{-1} and are generally stronger over the center and off Greenland as compared to the western channel off Canada's Ellesmere Island.

I find the same lateral ice velocity distribution for the second 2007–09 period of observation (Fig. 8). Note the abrupt change in ice draft in February 2009 after a northern ice arch forms (Fig. 3). A southern ice arch never forms in 2009 and all thick ice is flushed out of Nares Strait and replaced by thin, mobile first-year ice

TABLE 2. Basic statistics of depth-averaged currents. Mean directions and ellipse orientations are in degrees positive counterclockwise from true east. The degrees of freedom (DOF) are determined as the ratio of the record length T and integral decorrelation time scale T_d .

Name	(km)	Year	Mean speed	Direction	Major/minor axis	Orientation	DOF
KS02	2.2	2003–06	6.7 ± 0.7	-126	6.1/1.0	-123	285
KS04	5.4	2007–09	7.9 ± 0.7	-121	6.6/2.1	-121	340
KS06	11.7	2007–09	13.4 ± 2.0	-117	7.9/3.6	-112	59
KS08	17.8	2007–09	9.7 ± 1.4	-120	6.8/3.9	-114	91
KS10	23.9	2003–06	6.6 ± 0.9	-123	7.3/3.1	-124	274
KS10	24.6	2007–09	7.4 ± 0.9	-124	6.9/4.2	-120	231
KS12	29.6	2003–06	4.8 ± 1.1	-109	9.9/3.2	-127	271
KS12	31.5	2007–09	1.1 ± 1.3	-97	13.4/3.1	-125	332
KS14	34.4	2003–06	4.4 ± 1.1	63	13.5/2.1	-119	555

until the failure of the northern ice arch in July 2009 marks the arrival of thicker ice from the Arctic Ocean to the north.

Almost 60% of the variance of along-channel ice motion correlates with the variance of the local winds ($r^2 = 0.6$). Figure 9 shows the complex (vector) correlation C_{xy} of wind with ice motions for the entire 2007–09 period as a function of lag. The largest correlation occurs at zero lag at an angle $\text{Dir}(C_{xy})$ of -10° that represents a clockwise rotation of the wind into the sea ice vector. Integrating the lagged autocorrelation of the ice velocity over all lags, I derive a decorrelation time scale of ~ 1 and ~ 10 days for the across- and along-

channel velocity components, respectively (Kundu and Allen 1976). Tidal oscillations are visible in along- but not across-channel autocorrelations. Harmonic analyses reveal phase-locked tidal ice velocities whose

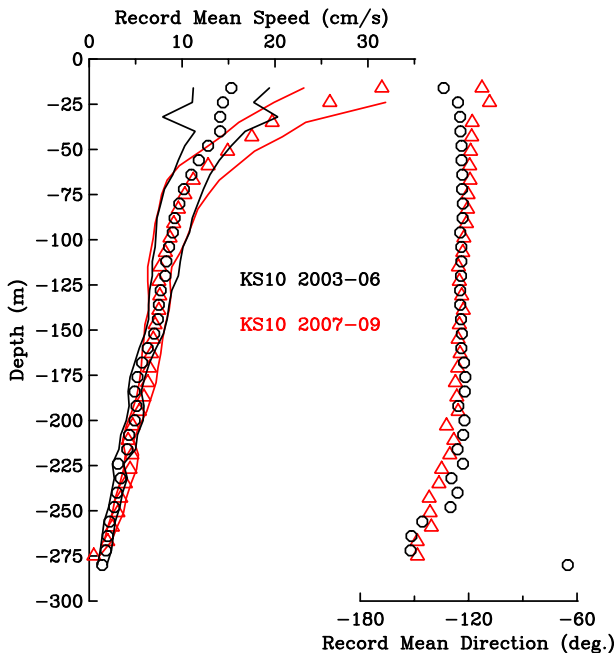


FIG. 5. Mean current speed and direction near the center of Kennedy Channel (KS10) for the 2003–06 and 2007–09 periods at all available depths. Uncertainties represent 95% confidence levels for speed; values at -16 and -24 m are from interpolating measured velocities into the surface layer using ice velocity estimates.

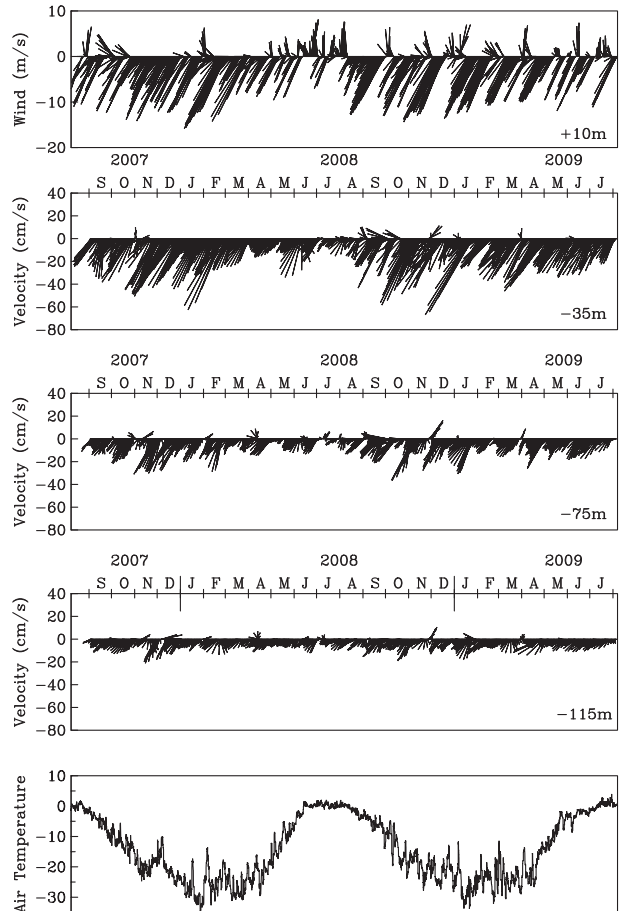


FIG. 6. Low-pass filtered time series of wind 10 m above and ocean current vectors at 25, 75, and 115 m below the surface as well as air temperature for the 2007–09 period. Wind and temperature ($^\circ\text{C}$) are from model predictions (Samelson and Barbour 2008), while ocean currents are from station KS10; see Figs. 4 and 5 for locations.

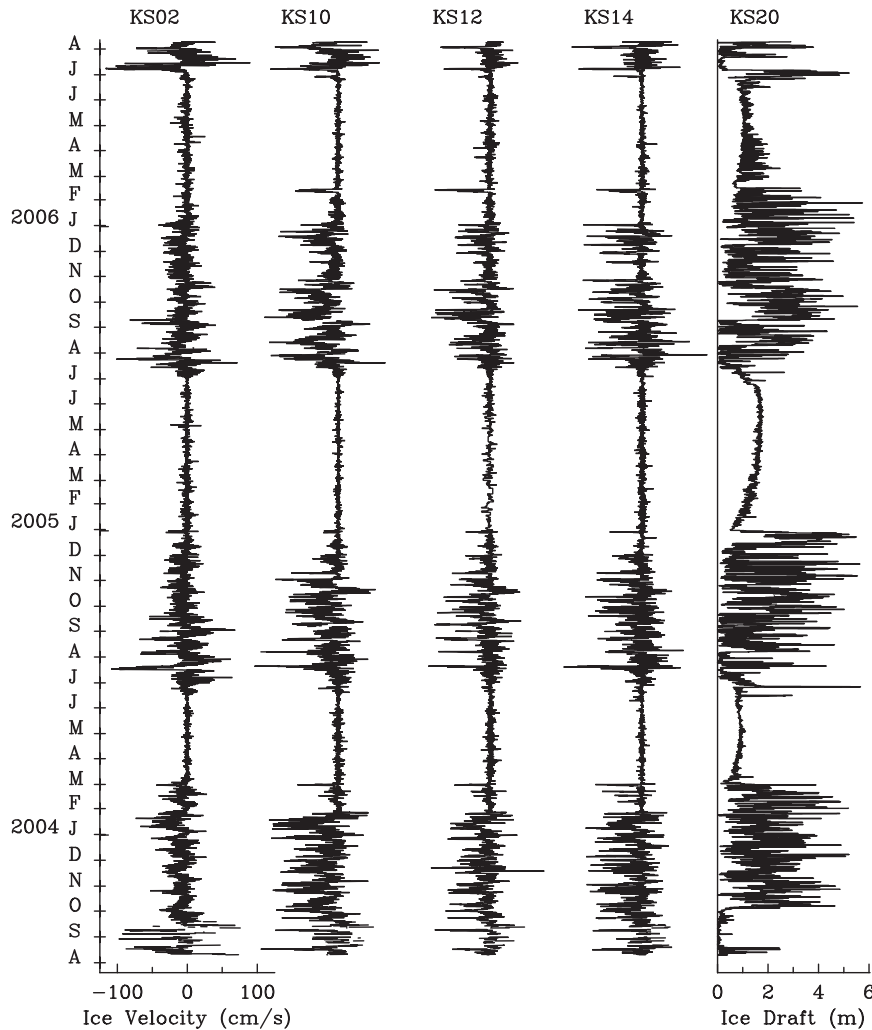


FIG. 7. Time series of ice velocity across Nares Strait from west (KS02) to east (KS14) with ice draft at KS20 for the 2003 to 2006 deployment.

amplitudes are about 60% of the tidal currents at 40-m below the surface (not shown).

c. Surface velocity

Subsurface ocean and ice velocity vectors are combined to estimate surface layer velocities via interpolation. More specifically, I interpolate velocity observations above 100-m depth toward the surface by fitting a constant (u_0, v_0) , a linear shear (u_1, v_1) , and an Ekman layer profile (u_E, v_E) to observations of along- and across-channel velocity components (u, v) . Both velocity components are fitted concurrently, that is,

$$u(z) = u_0 + u_1 z + v_E s(z) + u_E c(z), \quad \text{and} \quad (1)$$

$$v(z) = v_0 + v_1 z + v_E c(z) - u_E s(z), \quad (2)$$

where z is the vertical distance from the surface scaled by the vertical Ekman layer depth $D = (2A_v/f)^{1/2} = 10$ m;

f is the Coriolis parameter; and $A_v = 7.2 \times 10^{-3} \text{ m}^2 \text{ s}^{-1}$ is the vertical eddy viscosity, while $s(z) = \sin(z)e^{-z}$ and $c(z) = \cos(z)e^{-z}$ are the functions used to describe the Ekman layer profile. The six free parameters (u_0, v_0) , (u_1, v_1) , and (u_E, v_E) are determined by minimizing the least squares errors for data from the top 100 m of the water column at each time step for each profile. The root-mean-square error varies between 3.3 and 4.6 cm s^{-1} . The largest errors always occur within 5 km of the Ellesmere Island coast (not shown). Münchow et al. (2007) applied a similar procedure to vessel-mounted ADCP observations and discusses both the sensitivity and the uncertainty of the method.

5. Salinity

Salinity observation from moored sensors reveals dramatically different structures in the 2003–06 observational

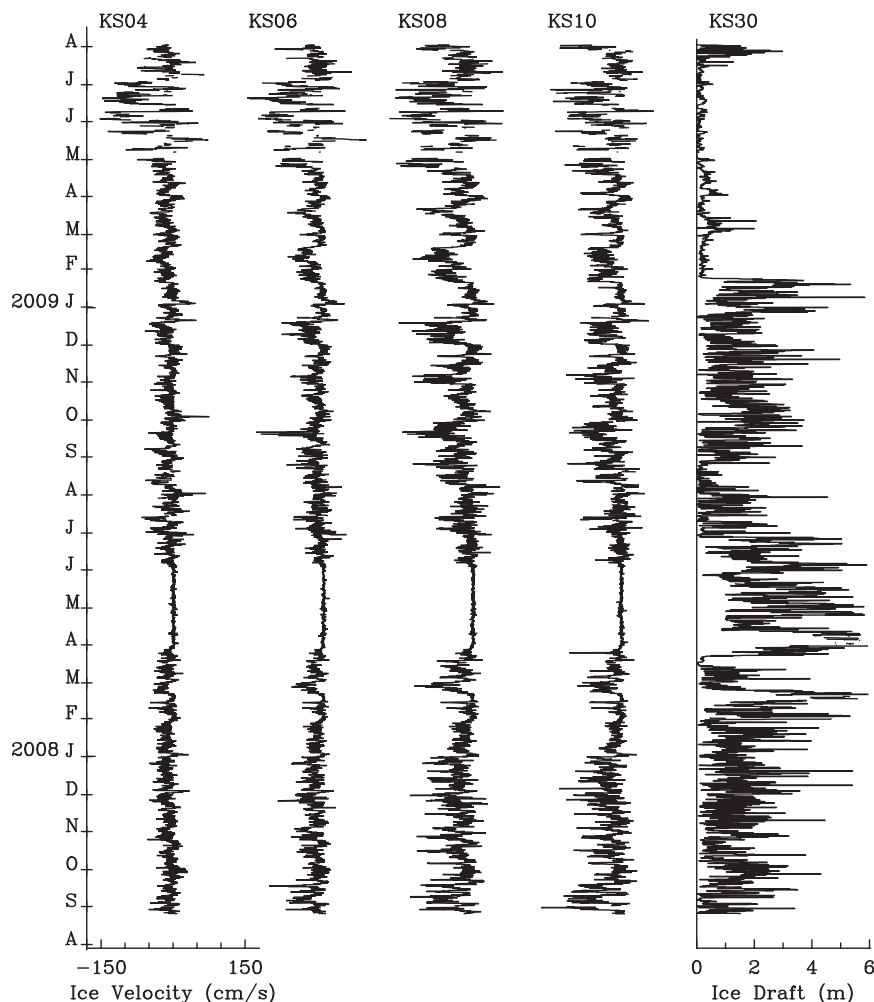


FIG. 8. Time series of ice velocity across Nares Strait from west (KS04) to east (KS10) with ice draft at KS30 for the 2007 to 2009 deployment.

period when it is compared to 2007–09 observations. Figures 10 and 11 show both the time-averaged and instantaneous salinity distributions across Nares Strait from moorings and ship-based summer profiling. Rabe et al. (2010, 2012) discuss the 2003–06 data in detail and estimate geostrophic flux below 30-m depth, respectively. Extending this methodology to the entire section, I here construct daily salinity distribution by assuming (i) a vertically uniform surface mixed layer with the time-varying salinity observed near 30-m depth; (ii) a time-varying observed vertical profile between 30- and 200-m depth; and (iii) a steady salinity distribution below 200 m where I use observed data from the summer surveys in 2003 and 2007 for all days.

Both the summer snapshots and interannual mean sections indicate isohalines that slope upward from Ellesmere Island in the west to Greenland in the east. This reflects the baroclinic contribution to the geostrophic circulation

(Rabe et al. 2012). Above 100-m depth, minimal salinities of about 32 occur near the center of the channel in 2003–06. In contrast, the 2007–09 salinity minima occur closer to the Ellesmere Island coast where record-mean surface salinities reach as low as 31, decreasing continuously from east to west. This response is consistent with a wind-forced surface circulation shown in Fig. 6 due to the mean winds to the south (Samelson and Barbour 2008). Recall that the second deployment period coincided with largely mobile ice conditions year-round.

6. Volume and freshwater flux

a. Flux definitions

Velocity and salinity fields $u(y, z, t)$ and $s(y, z, t)$ are decomposed into two components, for example, $u = U + u'$ and $s = S + s'$, where $U(y, z)$ and $S(y, z)$ are time-mean

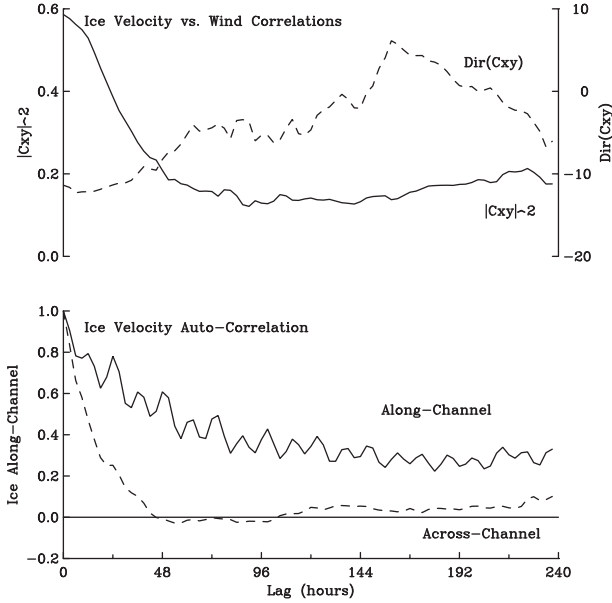


FIG. 9. (top) Time-lagged correlation of wind with ice velocity vector for the entire 2007 to 2009 deployment. Ice velocities are the across-channel average from five locations. Negative direction $\text{Dir}(C_{xy})$ indicates that the ice vector is rotated clockwise relative to the wind vector. C_{xy}^2 indicates the fraction of correlated variance. (bottom) The time-lagged autocorrelation of along (black) and across-channel (red) ice velocity.

fields with temporal fluctuations $u'(y, z, t)$ and $s'(y, z, t)$. The time average $\langle \cdot \rangle$ of the fluctuations is zero by construction, that is, $\langle u' \rangle = \langle s' \rangle = 0$, while $\langle u \rangle = U$ and $\langle s \rangle = S$. The mean volume flux $\langle Q(t) \rangle$ is then defined as

$$\langle Q(t) \rangle = \iint_A U \, dy \, dz, \quad (3)$$

where the integral is over the area $A = 10.59 \text{ km}^2$ of the section (y, z) in contact with water. The measurements are interpolated onto a regular grid with $dz = 4\text{-m}$ and $dy = 6\text{-km}$ spacing over a 400-m vertical and 36-km lateral domain using a biharmonic spline interpolation as implemented in the general mapping tools routine “surface” (Smith and Wessel 1990; Wessel 2009). Sandwell (1987) shows that it is mathematically equivalent to minimize the curvature. It thus results in an optimally smooth interpolated field consistent with the data. McIntosh (1990) discusses its relation to other equally “objective” mapping algorithms that minimize a prescribed but often poorly known error covariance function (Bretherton et al. 1976). The unknown interpolation error of the adopted data interpolation scheme using continuous curvature splines in tension is contained within the random errors of velocity and salinity of the uncertainty estimates discussed in section 6c.

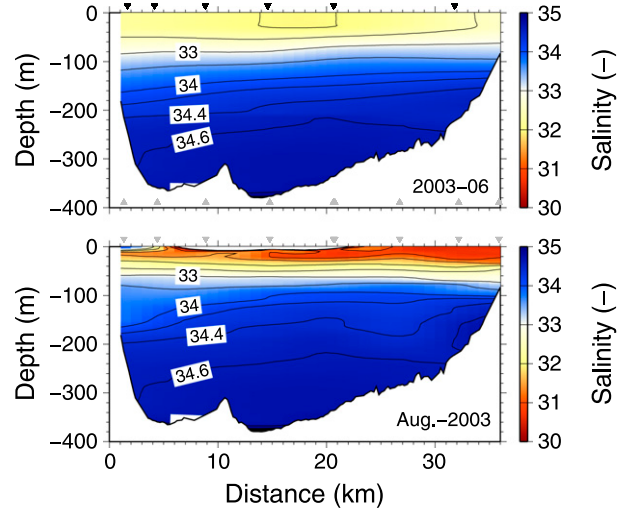


FIG. 10. Salinity across Kennedy Channel section of Nares Strait from (top) 2003–06 moorings (record mean) and (bottom) August 2003 CTD profiling (snapshot). Mooring locations are indicated by black triangles, while CTD profile locations are by gray symbols. View is to the north with Ellesmere Island on the left and Greenland on the right. Salinity has no units.

The flux of ocean freshwater $Q_f(t)$ combines along-channel velocity u with salinity anomaly $(s - S_0)/S_0$ that for the time mean Q_{f0} becomes

$$\begin{aligned} Q_{f0} &= \langle Q_f(t) \rangle = \left\langle \iint_A u(s/S_0 - 1) \, dy \, dz \right\rangle \\ &= \iint_A U(S/S_0 - 1) \, dy \, dz + \left\langle \iint_A u's'/S_0 \, dy \, dz \right\rangle \end{aligned} \quad (4)$$

for a reference salinity S_0 taken as 34.8. The gridding details are identical to those of volume flux, but uncertainty

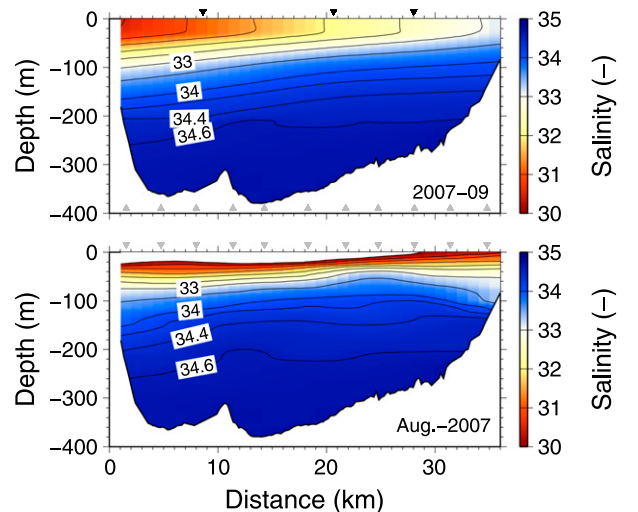


FIG. 11. As in Fig. 10, but for the (top) 2007–09 moorings and (bottom) August 2007 CTD. White areas near the surface are salinities less than 30.

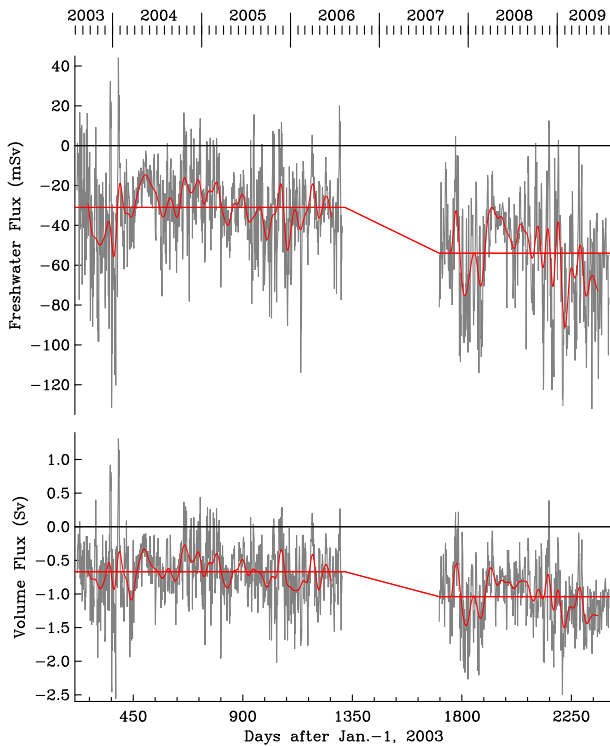


FIG. 12. (top) Freshwater and (bottom) volume flux through Nares Strait from August 2003 to July 2009 at daily (gray) and monthly (red) time scales. The mean flux for 2003–06 and 2007–09 are indicated in red; no data were collected from 2006 to 2007.

estimates for freshwater flux contain contributions from both velocity and salinity. The time average of the second term is negligible only if velocity and salinity fluctuations are orthogonal. Many observation-based Arctic freshwater flux numbers assume this contribution to be negligible because data to evaluate them are rarely available. In contrast, our daily velocity and salinity estimates from moored observations reveal that the second term never exceeds 0.8 mSv ($1 \text{ mSv} \equiv 10^3 \text{ m}^3 \text{ s}^{-1}$) and thus falls within our flux uncertainty estimates.

b. Daily flux time series

Using daily salinity and velocity data from moorings, I apply the same objective gridding procedures to evaluate $Q(t)$ and $Q_f(t)$. Figure 12 shows the resulting time series as well as its low-pass filtered, roughly monthly component thereof. The temporal mean flux increases by 68% from 32 mSv ($1053 \text{ km}^3 \text{ yr}^{-1}$) in 2003–06 to 54 mSv ($1780 \text{ km}^3 \text{ yr}^{-1}$) in 2007–09 (Table 3). Only the first value compares favorably to the geostrophic estimate of 28 mSv ($921 \text{ km}^3 \text{ yr}^{-1}$) for the same section and period (Rabe et al. 2012). The likely cause for this dramatic increase relates to the almost year-round mobile ice seasons in 2007–09. In most years a persistent ice arch across southern Smith Sound blocks ice motion throughout

Nares Strait for 4–6 months each winter (Kwok et al. 2010). In contrast, ice was mobile for the 2007–09 period except for 6 weeks in 2008 as indicated in Figs. 2 and 8.

While daily flux estimates range from -2.5 Sv (southward) to $+1.2 \text{ Sv}$ (northward) for volume and -130 to 45 mSv for freshwater, monthly flux values are always to the south (Fig. 12). Furthermore, flux exhibits little seasonality even though the largest southward freshwater flux occurs during December and January of each year except in 2004/05. The standard deviation about the respective mean flux is similar for the two observational periods, about 21 versus 26 mSv for freshwater and 0.44 Sv for volume (Fig. 12).

Volume and freshwater flux correlate strongly as 76% and 74% of the variances relate to each other for the 2003–06 and 2007–09 periods, respectively. Figure 13 shows this correlation as well as the corresponding linear regression, that is, each Sverdrup of volume flux accounts for 40 ± 1.4 and $51 \pm 2.1 \text{ mSv}$ of freshwater flux for the two periods. The uncertainties are 95% confidence limits in multiple regressions (Fofonoff and Bryden 1975) that indicate significantly different gains from the first to the second period. Volume flux estimates for Nares Strait can be used to estimate freshwater flux to within 25% at daily time scales.

c. Mean flux and random uncertainty

Figures 14 and 15 show the distribution of the record-mean along-channel currents U for the 2003–06 and 2007–09 periods, respectively, as well as $U(S/S_0 - 1)$. A surface-intensified high-velocity core occupies the center of the channel where southward speeds reach 0.4 m s^{-1} about 15 km from the coast off Ellesmere Island. The mean flow reduces to 0.1 m s^{-1} off Ellesmere Island, while within about 10 km off Greenland the mean surface flow is close to zero. Northward flows only occur within 3 km off Greenland where they reach 0.05 m s^{-1} in water 100 m deep. The flow within 200 m of the bottom elsewhere in the section is to the south and varies between 0.05 and 0.1 m s^{-1} .

The mean volume flux $\langle Q \rangle \pm \delta$ is $0.71 \pm 0.06 \text{ Sv}$ and $1.03 \pm 0.07 \text{ Sv}$ for the 2003–06 and 2007–09 periods, respectively. The uncertainty δ is a 95% confidence level due to a random velocity uncertainty of $\delta u = 0.01 \text{ m s}^{-1}$ to represent both measurement and interpolation error, that is,

$$\delta = 1.96 \times \sqrt{\frac{\left(\iint_A \delta u \, dy \, dz \right)^2}{N - 1}}, \quad (5)$$

where the degrees of freedom are $N - 1$. I conservatively assume here that each ADCP mooring location with 15 to 39 time series represents two independent

TABLE 3. Record-mean flux estimates for volume Q and freshwater Q_f . Uncertainties are 95% confidence limits that include random and interpolation errors; uncertainties in parentheses also include a systematic error due to a 20% uncertainty in surface ice velocity estimation. Values for Lancaster Sound and Davis Strait are from 1998 to 2006 (Peterson et al. 2012) and from 2004 to 2010 (Curry et al. 2014).

Year	Q (Sv)	Q_f Ocean (mSv)	Q_f Ice (mSv)
Nares Strait 2003–06	0.71 ± 0.06 (± 0.09)	32 ± 2.5 (± 5.7)	6.7 ± 0.33 (± 1.7)
Nares Strait 2007–09	1.03 ± 0.07 (± 0.11)	54 ± 3.9 (± 9.3)	9.8 ± 0.25 (± 2.2)
Lancaster Sound	0.53 ± 0.13	32 ± 6.0	2.1
Davis Strait 2004–10	1.6 ± 0.2	93 ± 6	10 ± 1

velocity estimates because the first two empirical orthogonal functions (not shown) generally explain 85% of the variance. Furthermore, the mooring array was designed to satisfy the Nyquist sampling theorem in both space and time that in practice results in a sample of correlated motions; that is, the number of independent, uncorrelated samples is smaller than the number of available time series by design. Mean across-channel velocities (not shown) are less than 10^{-3} m s^{-1} when averaged over the section.

The record-mean freshwater flux increases from $32 \pm 2.5 \text{ mSv}$ for the 2003–06 to $54 \pm 3.9 \text{ mSv}$ for the 2007–09 periods. Uncertainties here are estimated from error propagation that for a linear product such as $u \times s$ is the sum of the errors due to velocity and salinity. Each contribution is estimated by an integral similar to Eq. (5). Random salinity and velocity uncertainty of $\delta s = 0.1$ and $\delta u = 0.01 \text{ m s}^{-1}$ result in freshwater flux uncertainties of 1.8 (2.0) mSv from velocity and 0.8 (1.9) mSv for salinity for the 2003–06 (2007–09) period.

Freshwater flux estimates are lower bounds because salinities at 30-m depth are assumed to characterize a uniform surface layer. Actual surface salinities decrease toward the surface at times when vertical salinity stratification exists in this upper layer. Data from CTD surveys demonstrate that such stratification exists during the short summer when sea ice melt contributes to vertical stratification (Figs. 10, 11).

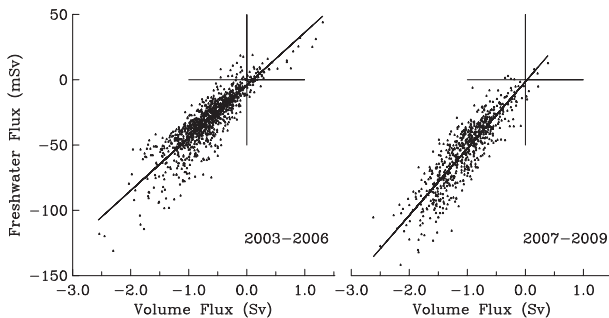


FIG. 13. Correlations (symbols) and regression (line) of freshwater vs volume flux. Note the different slopes for 2003–06 ($40 \pm 1.4 \text{ mSv Sv}^{-1}$) and 2007–09 ($51 \pm 2.1 \text{ mSv Sv}^{-1}$) regressions.

d. Surface layer flux and systematic errors

Table 3 summarizes record-mean fluxes along with their random and systematic errors. While random errors decline as the number of observations increases, systematic errors do not. One rarely discussed potential systematic error in flux estimates relates to the treatment of generally unmeasured velocity and salinity in a surface layer. In this study, flux values include interpolated surface velocity and extrapolated surface salinity estimates. Evaluating the impact of the surface layer, I construct flux estimates that exclude an increasing fraction of the surface layer from integrals such as Eqs. (3) and (4). Figure 16 then shows how much of the flux is contained within the excluded surface layer that is varied from zero to 30 m. Volume and freshwater flux are normalized by the full-section value given in Table 3.

Observations from Nares Strait suggest that more than 50% of the freshwater and more than 20% of the

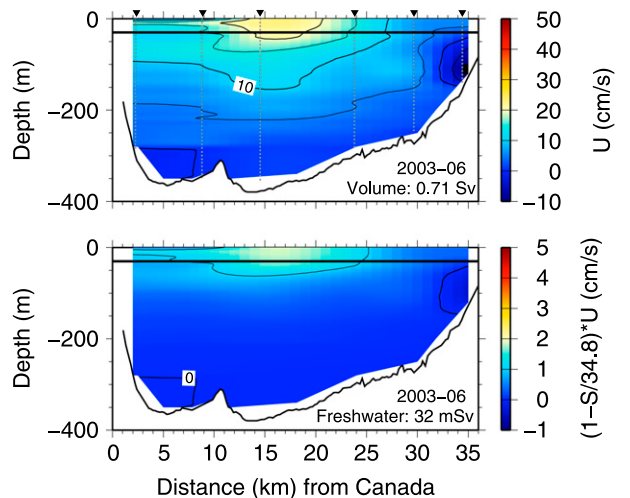


FIG. 14. (top) Record-mean flow and (bottom) freshwater flux per unit area for 2003–06 in the along-channel direction defined as 120° clockwise from true east. View is to the north with Greenland on the right and Canada on the left. Black symbols indicate mooring locations. Contours above the thick black line at $z = -30 \text{ m}$ separate direct observations from estimated values using Ekman layer function fitting. Positive flow is toward the southwest.

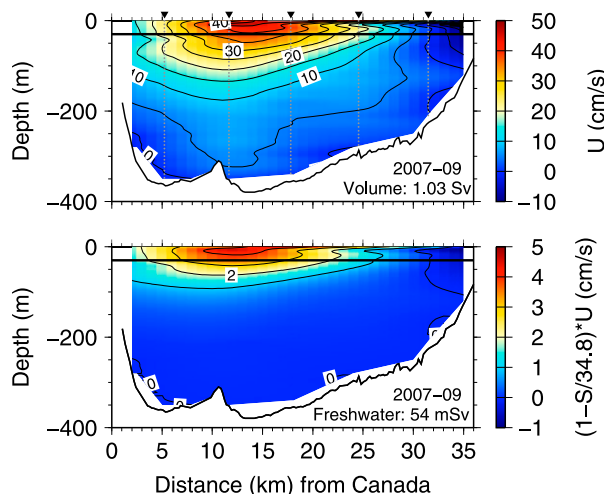


FIG. 15. As in Fig. 14, but for 2007–09.

volume flux are contained within 30 m of the surface. This estimate reflects data from multiple seasons and multiple years when the ice is mobile, landfast, or not present. These large flux contributions from an unmeasured surface layer imply potentially large systematic error that depends on how observations are extended into this surface layer. For example, if ice velocity estimates are consistently high or low by 20%, say, then this introduces a small error for volume flux (4% or ~ 0.04 Sv), but it will introduce a large error for freshwater flux (10% or ~ 5 mSv) because the freshwater flux is more sensitive to surface velocity than is volume flux. Table 3 presents both the random and the random plus systematic error for all record-mean flux estimates.

7. Wind and pressure gradient forcing

Winds drive ocean circulation both locally via a surface wind stress and remotely via horizontal pressure gradients (Garvine 1985). For local winds to drive ocean currents in ice-covered seas, however, the ice must be sufficiently mobile to allow the transfer of momentum. Sizeable ice velocities appear during the 2007–09 period at all times, except for April and May of 2008 (Fig. 8), which drive ice and oceans below. Figure 9 shows correlations of wind with ice velocity vectors and demonstrates the dominance of local winds in Nares Strait sea ice motions at daily time scales when ice is mobile.

In contrast, along-channel pressure gradient forcing of the ocean does not depend on ice cover or motion. Deriving an estimate of this pressure gradient, I use the difference of bottom pressure recordings from a northern and southern station and remove the record-mean

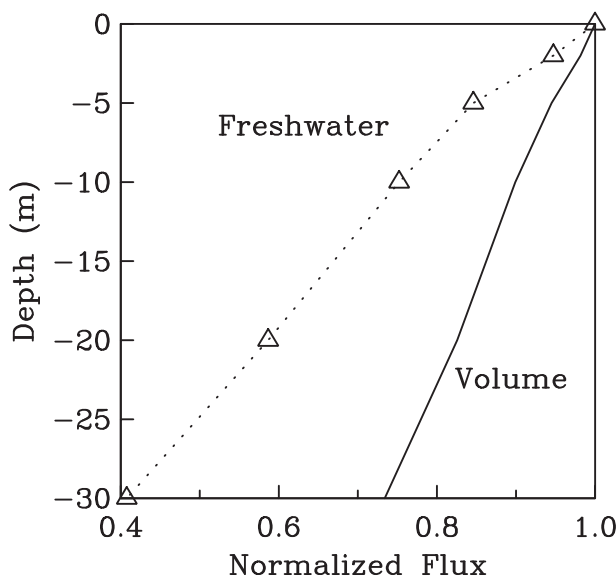


FIG. 16. Volume (solid line) and freshwater (dotted line with symbols) flux estimates in the surface layer normalized by the surface value. The upper limit of the sectional integral is the depth for which the integrated flux estimate is shown.

pressure. Münchow and Melling (2008) use identical data for a frequency–domain correlation analysis that reveals maximal correlation $r^2 \sim 0.8$ near a monthly time scale at zero lag well above the 95% confidence level of frequency–domain significance testing. Figure 17 shows the time series of pressure gradient and volume flux that are low-passed filtered with a Lanczos raised cosine filter that has a half-power point near 2 weeks. The difference in sea level pressure difference dP along the 450-km-long Nares Strait varies by about ± 0.1 m, while volume flux Q varies in the range from zero to 1.8 Sv to the south. A fraction of these data are used in the regression

$$Q = a + b dP, \quad (6)$$

where Q and dP from the first year are used to find coefficients $a = -0.92 \pm 0.023$ Sv and $b = 9.0 \pm 0.66$ Sv m^{-1} for the remainder of the time series. The uncertainties are 95% confidence limits in multiple linear regressions (Fofonoff and Bryden 1975). I then compare volume flux predictions $Q_p = a + b dP$ with volume flux observations Q and show the results in Fig. 17. The agreement of this simple forecasting model is excellent as the residuals are always less than 0.5 Sv with a root-mean-square error of 0.2 Sv. Figure 18 shows both the regression and the scatter of the data. The correlation between the two time series is 0.82; that is, 68% of the volume flux variance relates to the variance in the pressure difference along Nares Strait.

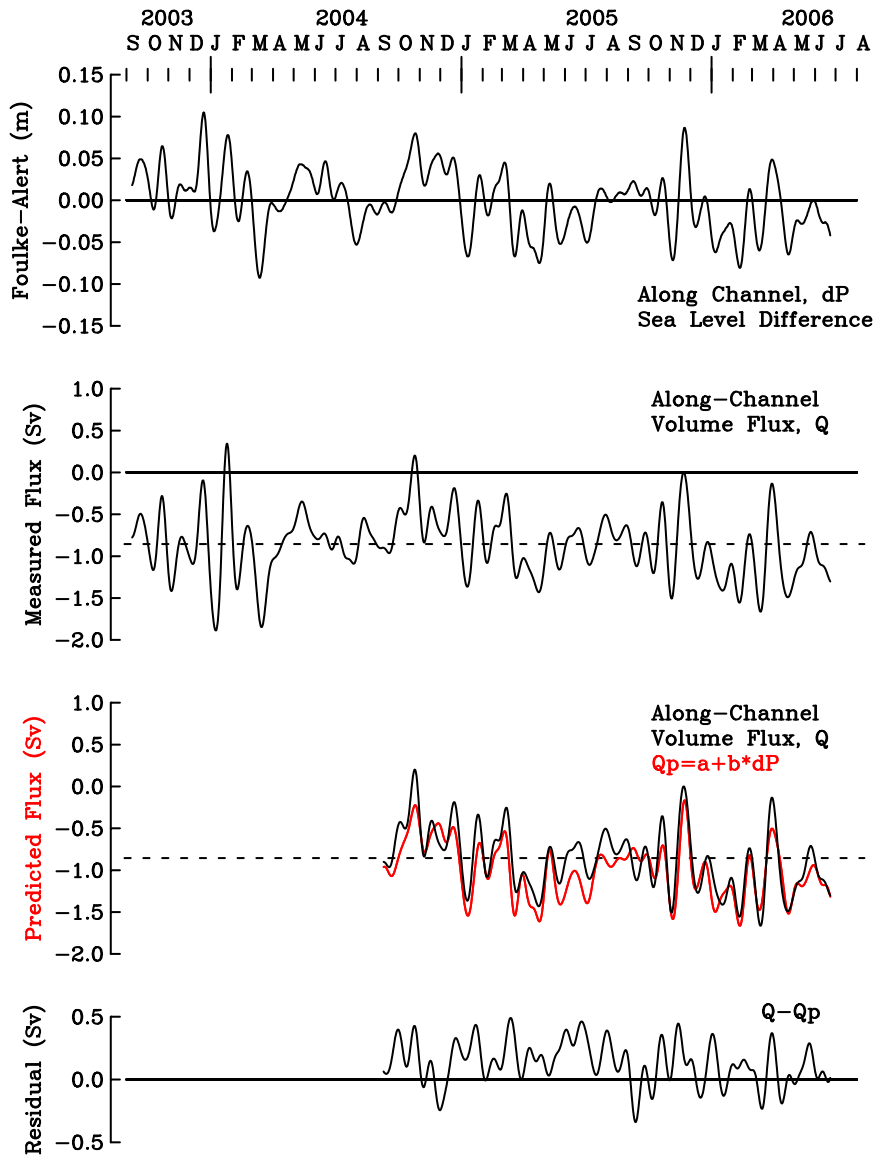


FIG. 17. (top panel) Regression of along-channel pressure difference between stations at Foulke Fjord and Alert with (second panel) volume flux across Kennedy Channel. (third panel) The prediction from the regression (red) is derived from the 2003/04 data and compared to the 2005/06 data (black).

8. Discussion and conclusions

Ice and ocean sensors deployed in Nares Strait between 2003 and 2009 quantified the export of volume and freshwater from the Arctic to the North Atlantic Oceans between northern Canada and Greenland. These data demonstrated dramatic change in all observed and estimated parameters from a first 2003–06 to a second 2007–09 study period. Both ice and ocean velocities increased in southward magnitude, while surface waters also became fresher. More specifically, volume flux increased by 45%, ocean freshwater flux increased by

69%, and ice freshwater flux increased by 46% from the first to the second period (Table 3).

These observed changes relate to different winter sea ice regimes during these two periods. Sea ice during the first 2003–06 period was motionless for 5–8 months of the year as the result of a southern ice arch that forms in late winter and collapses in early summer (Kwok et al. 2010). This ice arch failed to form in the winters of 2006/07, 2007/08, and 2009/10, while it existed for less than 2 months in 2008/09.

While Kwok et al. (2010) documents these first recorded failures using remotely sensed ice properties, this study quantifies how changes in winter ice regime

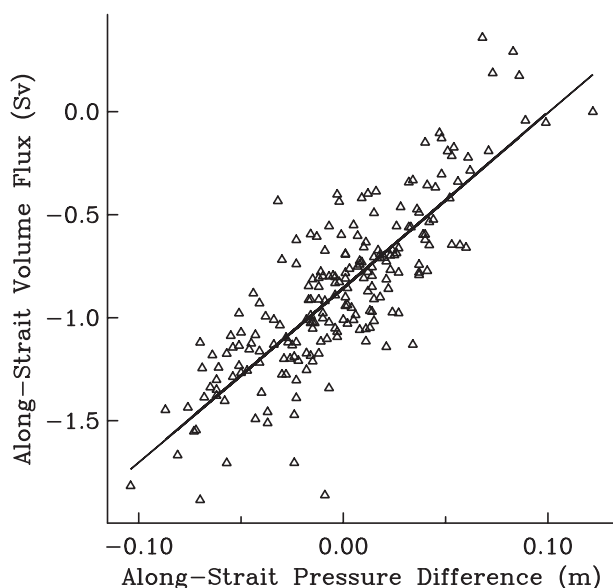


FIG. 18. Correlation ($r^2 = 0.68$) and regression of along-channel pressure difference dP with volume flux Q .

impact ocean volume and liquid freshwater flux. More specifically, the new regime without a southern ice arch facilitates larger flux in winter, enhances momentum transfer via coupled ice–ocean motions, results in an “earlier” open-water season, and allows enhanced solar heating. These changes all increase the time window that thick Arctic ice can stream southward through Nares Strait in summer, partially melt in transit in Nares Strait, and thus freshen ocean surface waters. Furthermore, when the sea ice cover is mobile, local wind forcing provides a more efficient momentum transfer from the atmosphere to the ocean.

All prior flux studies of Nares Strait were limited to observations below 30-m depth (Münchow and Melling 2008; Rabe et al. 2012) or were based on daily snapshots of survey data (Münchow et al. 2007). In contrast, this study provided daily flux estimates for the complete section by interpolating observations into the 30-m surface layer using ice velocities that were derived from the same ADCPs that measured water column velocities (Melling et al. 1995; Visbeck and Fischer 1995). Statistical analyses of these ice velocities reveal both tidal oscillations as well as strong correlations with the local winds at a 10° angle at zero lag. This gives confidence that both ice and surface velocity estimates are accurate and physically meaningful.

Furthermore, the complete 2003–09 dataset includes a second period of observations that differs qualitatively and quantitatively from the prior 2003–06 record. I thus conclude that present flux estimates are more robust, complete, and comprehensive. All freshwater flux estimates

contain uncertainty estimates that incorporate contributions from random velocity and salinity errors as well as a potential systematic error from the surface layer interpolation.

Along-channel bottom pressure gradients explain 68% of the volume flux for the 2003–06 period that includes periods with and without ice motions. Furthermore, about 75% of the freshwater flux variance relates linearly to the volume flux variance for both 2003–06 and 2007–09 periods, even though the gain of volume to freshwater flux differs. These analyses suggest that two tide gauges or bottom pressure sensors placed at the northern entrance and southern exit of Nares Straits may capture 60% of freshwater flux variability. The expensively acquired measurements of this study thus provide the basis for an inexpensive monitoring array.

The coupling of Arctic to North Atlantic Oceans in Nares Strait to the west of Greenland depends on the mobility of the sea ice cover. While along-channel pressure gradients dominate the ocean flow irrespectively of the ice cover, the flux of freshwater is increased by almost 70% during years when the sea ice is mobile in winter. Incidentally, the large-scale general circulation climate model of Koenigk et al. (2007) predicts an increase of liquid freshwater flux through the Canadian Archipelago by 38% from 80 to 110 mSv for the second half of the twenty-first century as a consequence of a warming world with diminished and more mobile sea ice cover (Stroeve et al. 2012).

The precise dynamics is unclear from an observational perspective, but I speculate that more efficient local momentum transfer from the wind field to the ocean plays a central role, as does the baroclinic adjustment of a boundary current along the Canadian Ellesmere Island coast that is caused by enhanced onshore surface Ekman flux. Only detailed process-oriented numerical studies motivated by observations and analyses will provide the dynamical understanding needed to make meaningful predictions into the future (Shroyer et al. 2015).

The southern ice arch formed again each winter 2010/11 through 2014/15 at its normal location for several months each year. The 2007–09 period may thus be regarded as an extreme anomaly caused by an intermittent release of Arctic freshwater from the Beaufort Gyre (Curry et al. 2014; Timmermans et al. 2011).

Acknowledgments. The National Science Foundation supported the initial fieldwork with OPP-0230236 and analyses with OPP-1022843. The University of Delaware provided substantial additional support with capital equipment and salaries. Instrument preparation, deployment, and recoveries were accomplished through dedicated efforts by a large group of international scientists, engineers,

technicians, students, and staff in addition to the captains and crews of multiple ships on multiple expeditions. Humfrey Melling of the Canadian Department of Fisheries and Oceans provided critical leadership and design ideas on all moored ocean sensor systems that were implemented creatively by Peter Gamble, David Huntley, Ron Lindsey, and Jonathan Poole. Pat Ryan processed ice draft data shown in Figs. 7 and 8. Comments by Benjamin Rabe and anonymous reviewers improved the manuscript.

REFERENCES

- Aagaard, K., and E. C. Carmack, 1989: The role of sea ice and other fresh water in the Arctic circulation. *J. Geophys. Res.*, **94**, 14 485–14 498, doi:10.1029/JC094iC10p14485.
- Alkire, M. B., K. K. Falkner, I. Rigor, M. Steele, and J. Morison, 2007: The return of Pacific waters to the upper layers of the central Arctic Ocean. *Deep-Sea Res.*, **54**, 1509–1529, doi:10.1016/j.dsr.2007.06.004.
- Belkin, I. M., 2004: Propagation of the “Great Salinity Anomaly” of the 1990s around the northern North Atlantic. *Geophys. Res. Lett.*, **31**, L08306, doi:10.1029/2003GL019334.
- Beszczynska-Möller, A., R. A. Woodgate, C. Lee, H. Melling, and M. Karcher, 2011: A synthesis of exchanges through the main oceanic gateways to the Arctic Ocean. *Oceanography*, **24**, 82–99, doi:10.5670/oceanog.2011.59.
- Bretherton, F. P., R. E. Davis, and C. B. Fandry, 1976: A technique for objective analysis and design of oceanographic experiments applied to MODE-73. *Deep-Sea Res. Oceanogr. Abstr.*, **23**, 559–582, doi:10.1016/0011-7471(76)90001-2.
- Bryden, H. L., H. R. Longworth, and S. A. Cunningham, 2005: Slowing of the Atlantic meridional overturning circulation at 25°N. *Nature*, **438**, 655–657, doi:10.1038/nature04385.
- Copland, L., D. R. Mueller, and L. Weir, 2007: Rapid loss of the Ayles Ice Shelf, Ellesmere Island, Canada. *Geophys. Res. Lett.*, **34**, L21501, doi:10.1029/2007GL031809.
- Curry, B., C. M. Lee, B. Petrie, R. E. Moritz, and R. Kwok, 2014: Multiyear volume, liquid freshwater, and sea ice transports through Davis Strait, 2004–10. *J. Phys. Oceanogr.*, **44**, 1244–1266, doi:10.1175/JPO-D-13-0177.1.
- Curry, R., and C. Mauritzen, 2005: Dilution of the northern North Atlantic Ocean in recent decades. *Science*, **308**, 1772–1774, doi:10.1126/science.1109477.
- de Steur, L., E. Hansen, R. Gerdes, M. Karcher, E. Fahrbach, and J. Holfort, 2009: Freshwater fluxes in the East Greenland Current: A decade of observations. *Geophys. Res. Lett.*, **36**, L23611, doi:10.1029/2009GL041278.
- Dickson, B., I. Yashayaev, J. Meincke, B. Turrell, S. Dye, and J. Holfort, 2002: Rapid freshening of the deep North Atlantic Ocean over the past four decades. *Nature*, **416**, 832–837, doi:10.1038/416832a.
- Dickson, R., B. Rudels, S. Dye, M. Karcher, J. Meincke, and I. Yashayaev, 2007: Current estimates of freshwater flux through Arctic and subarctic seas. *Prog. Oceanogr.*, **73**, 210–230, doi:10.1016/j.pocan.2006.12.003.
- Emile-Geay, J., M. A. Cane, N. Naik, R. Seager, A. C. Clement, and A. van Geen, 2003: Warren revisited: Atmospheric freshwater fluxes and “Why is no deep water formed in the North Pacific.” *J. Geophys. Res.*, **108**, 3178, doi:10.1029/2001JC001058.
- Fofonoff, N., and H. Bryden, 1975: Density of sea waters. *J. Mar. Res.*, **41**, 69–82.
- Garvine, R. W., 1985: A simple model of estuarine subtidal fluctuations forced by local and remote wind stress. *J. Geophys. Res.*, **90**, 11 945–11 948, doi:10.1029/JC090iC06p11945.
- Greene, C., J. Pershing, T. Cronin, and N. Ceci, 2008: Arctic climate change and its impacts on the ecology of the North Atlantic. *Ecology*, **89**, S24–S38, doi:10.1890/07-0550.1.
- Haine, T. W. N., and Coauthors, 2015: Arctic freshwater export: Status, mechanisms, and prospects. *Global Planet. Change*, **125**, 13–35, doi:10.1016/j.gloplacha.2014.11.013.
- Holland, M. M., J. Finnis, A. P. Barrett, and M. C. Serreze, 2007: Projected changes in Arctic Ocean freshwater budgets. *J. Geophys. Res.*, **112**, G04S55, doi:10.1029/2006JG000354.
- Hurrell, J. W., and C. Deser, 2009: North Atlantic climate variability: The role of the North Atlantic Oscillation. *J. Mar. Syst.*, **78**, 28–41, doi:10.1016/j.jmarsys.2008.11.026.
- Jahn, A., and Coauthors, 2012: Arctic Ocean freshwater: How robust are model simulations? *J. Geophys. Res.*, **117**, C00D16, doi:10.1029/2012JC007907.
- Johnson, H., A. Münchow, K. Falkner, and H. Melling, 2011: Ocean circulation and properties in Petermann Fjord, Greenland. *J. Geophys. Res.*, **116**, C01003, doi:10.1029/2010JC006519.
- Khatiwala, S. P., R. G. Fairbanks, and R. W. Houghton, 1999: Freshwater sources to the coastal ocean off northeastern North America: Evidence from ¹⁸O/H₂¹⁶O. *J. Geophys. Res.*, **104**, 18 241–18 255, doi:10.1029/1999JC900155.
- Koenigk, T., U. Mikolajewicz, H. Haak, and J. Jungclauss, 2007: Arctic freshwater export in the 20th and 21st centuries. *J. Geophys. Res.*, **112**, G04S41, doi:10.1029/2006JG000274.
- Kundu, P., and J. Allen, 1976: Some three-dimensional characteristics of low-frequency current fluctuations near the Oregon coast. *J. Phys. Oceanogr.*, **6**, 181–199, doi:10.1175/1520-0485(1976)006<0181:STDCOL>2.0.CO;2.
- Kwok, R., and D. A. Rothrock, 2009: Decline in Arctic sea ice thickness from submarine and ICESat records: 1958–2008. *Geophys. Res. Lett.*, **36**, L15501, doi:10.1029/2009GL039035.
- , L. T. Pedersen, P. Gudmandsen, and S. S. Pang, 2010: Large sea ice outflow into the Nares Strait in 2007. *Geophys. Res. Lett.*, **37**, L03502, doi:10.1029/2009GL041872.
- LeBlond, P. H., 1980: On the surface circulation in some channels of the Canadian Arctic Archipelago. *Arctic*, **33**, 189–197, doi:10.14430/arctic2554.
- Lindsay, R. W., J. Zhang, A. Schweiger, M. Steele, and H. Stern, 2009: Arctic sea ice retreat in 2007 follows thinning trend. *J. Climate*, **22**, 165–176, doi:10.1175/2008JCLI2521.1.
- Lu, Y. Y., S. Hoggins, S. Nudds, S. Prinsenber, and G. Garric, 2014: Model simulated volume fluxes through the Canadian Arctic Archipelago and Davis Strait: Linking monthly variations to forcing in different seasons. *J. Geophys. Res. Oceans*, **119**, 1927–1942, doi:10.1002/2013JC009408.
- McGeehan, T., and W. Maslowski, 2012: Evaluation and control mechanisms of volume and freshwater export through the Canadian Arctic Archipelago in a high-resolution pan-Arctic ice-ocean model. *J. Geophys. Res.*, **117**, C00D14, doi:10.1029/2011JC007261.
- McIntosh, P. C., 1990: Oceanographic data interpolation: Objective analysis and splines. *J. Geophys. Res.*, **95**, 13 529–13 541, doi:10.1029/JC095iC08p13529.

- Melling, H., 1998: Sound scattering from sea ice: Aspects relevant to ice-draft profiling by sonar. *J. Atmos. Oceanic Technol.*, **15**, 1023–1034, doi:10.1175/1520-0426(1998)015<1023:SSFSIA>2.0.CO;2.
- , P. Johnston, and D. Riedel, 1995: Measurements of the underside topography of sea ice by moored subsea sonar. *J. Atmos. Oceanic Technol.*, **12**, 589–602, doi:10.1175/1520-0426(1995)012<0589:MOTUTO>2.0.CO;2.
- , Y. Gratton, and G. Ingram, 2001: Ocean circulation within the North Water polynya of Baffin Bay. *Atmos.–Ocean*, **39**, 301–325, doi:10.1080/07055900.2001.9649683.
- , and Coauthors, 2008: Fresh-water fluxes via Pacific and Arctic outflows across the Canadian polar shelf. *Arctic–Subarctic Ocean Fluxes*, R. R. Dickson, J. Meincke, and P. Rhines, Eds., Springer, 193–247.
- Morison, J., M. Steele, and R. Andersen, 1998: Hydrography of the upper Arctic Ocean measured from the nuclear submarine U.S.S. *Pargo*. *Deep-Sea Res.*, **45**, 15–38, doi:10.1016/S0967-0637(97)00025-3.
- Münchow, A., and H. Melling, 2008: Ocean current observations from Nares Strait to the west of Greenland: Interannual to tidal variability and forcing. *J. Mar. Res.*, **66**, 801–833, doi:10.1357/002224008788064612.
- , —, and K. K. Falkner, 2006: An observational estimate of volume and freshwater flux leaving the Arctic Ocean through Nares Strait. *J. Phys. Oceanogr.*, **36**, 2025–2041, doi:10.1175/JPO2962.1.
- , K. K. Falkner, and H. Melling, 2007: Spatial continuity of measured seawater and tracer fluxes through Nares Strait, a dynamically wide channel bordering the Canadian Archipelago. *J. Mar. Res.*, **65**, 759–788, doi:10.1357/002224007784219048.
- , —, B. Rabe, and H. L. Johnson, 2011: Ocean warming of Nares Strait bottom waters off northwest Greenland, 2003–2009. *Oceanography*, **24**, 114–123, doi:10.5670/oceanog.2011.62.
- , —, and —, 2015: Baffin Island and West Greenland Current systems in northern Baffin Bay. *Prog. Oceanogr.*, **132**, 305–317, doi:10.1016/j.pocean.2014.04.001.
- Myers, P. G., 2005: Impact of freshwater from the Canadian Arctic Archipelago on Labrador Sea Water formation. *Geophys. Res. Lett.*, **32**, L06605, doi:10.1029/2004GL022082.
- Parkinson, C. L., and D. J. Cavalieri, 2008: Arctic sea ice variability and trends, 1979–2006. *J. Geophys. Res.*, **113**, C07003, doi:10.1029/2007JC004558.
- Peterson, B. J., R. M. Holmes, J. W. McClelland, C. J. Vorosmarty, R. B. Lammers, A. I. Shiklomanov, I. A. Shiklomanov, and S. Rahmstorf, 2002: Increasing river discharge to the Arctic Ocean. *Science*, **298**, 2171–2173, doi:10.1126/science.1077445.
- Peterson, I., J. Hamilton, S. Prinsenberg, and R. Pettipas, 2012: Wind-forcing of volume transport through Lancaster Sound. *J. Geophys. Res.*, **117**, C11018, doi:10.1029/2012JC008140.
- Polyakov, I. V., and Coauthors, 2008: Arctic Ocean freshwater changes over the past 100 years and their causes. *J. Climate*, **21**, 364–384, doi:10.1175/2007JCLI1748.1.
- Proshutinsky, A., and Coauthors, 2009: Beaufort Gyre freshwater reservoir: State and variability from observations. *J. Geophys. Res.*, **114**, C00A10, doi:10.1029/2008JC005104.
- Rabe, B., A. Münchow, H. Johnson, and H. Melling, 2010: Nares Strait hydrography and salinity field from a 3-year moored array. *J. Geophys. Res.*, **115**, C07010, doi:10.1029/2009JC005966.
- , H. Johnson, A. Münchow, and H. Melling, 2012: Geostrophic currents and freshwater fluxes through Nares Strait to the west of northern Greenland. *J. Mar. Res.*, **70**, 603–640, doi:10.1357/002224012805262725.
- , and Coauthors, 2013: Liquid export of Arctic freshwater components through the Fram Strait 1998–2011. *Ocean Sci.*, **9**, 91–109, doi:10.5194/os-9-91-2013.
- , and Coauthors, 2014: Arctic Ocean basin liquid freshwater storage trend 1992–2012. *Geophys. Res. Lett.*, **41**, 961–968, doi:10.1002/2013GL058121.
- Rignot, E., and K. Steffen, 2008: Channelized bottom melting and stability of floating ice shelves. *Geophys. Res. Lett.*, **35**, L02503, doi:10.1029/2007GL031765.
- Rigor, I. G., J. M. Wallace, and R. L. Colony, 2002: Response of sea ice to the Arctic oscillation. *J. Climate*, **15**, 2648–2663, doi:10.1175/1520-0442(2002)015<2648:ROSITT>2.0.CO;2.
- Sadler, H., 1976: Water, heat, and salt transport through Nares Strait, Ellesmere Island. *J. Fish. Res. Board Can.*, **33**, 2286–2295, doi:10.1139/f76-275.
- Samelson, R., and P. Barbour, 2008: Low-level winds in Nares Strait: A model-based mesoscale climatology. *Mon. Wea. Rev.*, **136**, 4746–4759, doi:10.1175/2007MWR2326.1.
- Sandwell, D. T., 1987: Biharmonic spline interpolation of GEOS-3 and SEASAT altimeter data. *Geophys. Res. Lett.*, **14**, 139–142, doi:10.1029/GL014i002p00139.
- Shroyer, E. L., R. M. Samelson, L. Padman, and A. Münchow, 2015: Modeled ocean circulation in Nares Strait and its dependence on landfast-ice cover. *J. Geophys. Res. Oceans*, doi:10.1002/2015JC011091, in press.
- Smith, W. H. F., and P. Wessel, 1990: Gridding with continuous curvature splines in tension. *Geophysics*, **55**, 293–305, doi:10.1190/1.1442837.
- Steffen, K., and A. Schweiger, 1991: NASA team algorithm for sea ice concentration retrieval from Defense Meteorological Satellite Program Special Sensor Microwave Imager: Comparison with Landsat satellite imagery. *J. Geophys. Res.*, **96**, 21 971–21 987, doi:10.1029/91JC02334.
- Stroeve, J. C., J. Maslanik, M. C. Serreze, I. Rigor, W. Meier, and C. Fowler, 2011: Sea ice response to an extreme negative phase of the Arctic Oscillation during winter 2009/2010. *Geophys. Res. Lett.*, **38**, L02502, doi:10.1029/2010GL045662.
- , M. C. Serreze, M. M. Holland, J. E. Kay, J. Malanik, and A. P. Barrett, 2012: The Arctic's rapidly shrinking sea ice cover: A research synthesis. *Climatic Change*, **110**, 1005–1027, doi:10.1007/s10584-011-0101-1.
- Sundby, S., and K. Drinkwater, 2007: On the mechanisms behind salinity anomaly signals of the northern North Atlantic. *Prog. Oceanogr.*, **73**, 190–202, doi:10.1016/j.pocean.2007.02.002.
- Timmermans, M. L., A. Proshutinsky, R. A. Krishfield, D. K. Perovich, J. A. Richter-Menge, T. P. Stanton, and J. M. Toole, 2011: Surface freshening in the Arctic Ocean's Eurasian basin: An apparent consequence of recent change in the wind-driven circulation. *J. Geophys. Res.*, **116**, C00D03, doi:10.1029/2011JC006975.
- Visbeck, M., and J. Fischer, 1995: Sea surface conditions remotely sensed by upward-looking ADCP. *J. Atmos. Oceanic Technol.*, **12**, 141–149, doi:10.1175/1520-0426(1995)012<0141:SSCRSB>2.0.CO;2.
- Wekerle, C., Q. Wang, S. Danilov, T. Jung, and J. Schroter, 2013: The Canadian Arctic Archipelago throughflow in a multi-resolution global model: Model assessment and the driving

- mechanism of interannual variability. *J. Geophys. Res. Oceans*, **118**, 4525–4541, doi:[10.1002/jgrc.20330](https://doi.org/10.1002/jgrc.20330).
- Wessel, P., 2009: A general-purpose Green's function-based interpolator. *Comput. Geosci.*, **35**, 1247–1254, doi:[10.1016/j.cageo.2008.08.012](https://doi.org/10.1016/j.cageo.2008.08.012).
- White, D., and Coauthors, 2007: The Arctic freshwater system: Changes and impacts. *J. Geophys. Res.*, **112**, G04S54, doi:[10.1029/2006JG000353](https://doi.org/10.1029/2006JG000353).
- Woodgate, R. A., T. J. Weingartner, and R. Lindsay, 2012: Observed increases in Bering Strait oceanic fluxes from the Pacific to the Arctic from 2001 to 2011 and their impacts on the Arctic Ocean water column. *Geophys. Res. Lett.*, **39**, L24603, doi:[10.1029/2012GL054092](https://doi.org/10.1029/2012GL054092).
- Wunsch, C., and P. Heimbach, 2006: Estimated decadal changes in the North Atlantic meridional overturning circulation and heat flux 1993–2004. *J. Phys. Oceanogr.*, **36**, 2012–2024, doi:[10.1175/JPO2957.1](https://doi.org/10.1175/JPO2957.1).
- Zweng, M. M., and A. Münchow, 2006: Warming and freshening of Baffin Bay, 1916–2003. *J. Geophys. Res.*, **111**, C07016, doi:[10.1029/2005JC003093](https://doi.org/10.1029/2005JC003093).